Electronic Supplementary Material (ESI) for Journal of Materials Chemistry A.
This journal is © The Royal Society of Chemistry 2020

Supporting Information

Towards the Understanding of Acetonitrile Suppressing Salt Precipitation Mechanism in Water-in-Salt Electrolyte for Low-temperature Supercapacitor

Yinglun Sun[a,b], Yue Wang[c], Lingyang Liu[a,b], Bao Liu [a,b], Qingnuan Zhang[a], Dandan Wu[d], Hongzhang Zhang[e] and Xingbin Yan[a,b,f]*

[a] Laboratory of Clean Energy Chemistry and Materials, Lanzhou Institute of Chemical Physics, Chinese Academy of Sciences, Lanzhou, 730000, China.

[b] Center of Materials Science and Optoelectronics Engineering, University of Chinese Academy of Sciences, Beijing 100049, China

[c] School of Physical Science and Technology, Lanzhou University, Lanzhou, 730000, China.

[d] Department of Physics, School of Science, Lanzhou University of Technology, Lanzhou, 730000, China.

[e] Dalian National Laboratory for Clean Energy, Dalian, 116023, China.

[f] International Academy of Optoelectronics at Zhaoqing, South China Normal University, Zhaoqing, 52600, China.

* Corresponding author. E-mail address: xbyan@licp.cas.cn

Table S1. The coordination numbers for Na-O※, Na-O=, and Na-N※ of $NaClO_4$-based solutions with different H_2O/ACN molar ratio.

solution	Number (ClO_4^-)	Number (H_2O)	Number (ACN)
$(NaClO_4)_{1.7}/(H_2O)_{5.5}$	2.77	3.24	0
$(NaClO_4)_{1.7}/(H_2O)_{4.7}(ACN)_2$	1.865	2.951	1.15
$(NaClO_4)_{1.7}/(H_2O)_{4.7}(ACN)_3$	1.522	2.866	1.568
$(NaClO_4)_{1.7}/(H_2O)_{4.7}(ACN)_4$	1.268	2.764	1.913

Table S2. The comparison of low-temperature electrochemical performance for aqueous supercapacitors.

Materials	Electrolyte	Potential window	Lowest operating temperature (LOT)	Specific capacitance (RT)	Specific capacitance (LOT)	C_{LOT}/C_{RT}	Rate capability (LOT)	cyclic stability (LOT)	Ref.
activated carbon	SA-g-DA/KCl hydrogel electrolyte (3 M KCl)	0.8 V	-10 °C	97 F g^{-1} (1.0 A g^{-1}) single electrode	79.5 F g^{-1} (1.0 A g^{-1}) single electrode	81.95%	-	99.37% after 1350 cycles	1
PEDOTS-RuO_2@PEDOTS	LiCl-PVA gel electrolyte (3.5 M LiCl)	1.5 V	-60 °C	179.8 mF cm^{-2} (50 mV s^{-1})	78.8 mF cm^{-2} (50 mV s^{-1})	43.82%	22.2% (from 5 to 100 mV S^{-1})	97.2% after 5000 cycles	2
activated carbon	$NaClO_4$ aqueous solution (5 M)	1.2 V	-30 °C	158 F g^{-1} (5 mV s^{-1}) single electrode	-	-		-	3
commercial graphene nanoplatelets	[BMIm]Cl/H_2O electrolyte with 0.1m 4hT (20 m)	2.5 V	-32°C	480 F g^{-1} (20 mV s^{-1}) single electrode	97 F g^{-1} (20 mV s^{-1}) single electrode	20.20%	29.9% (from 20 to 400 mV s^{-1})	-	4
porous carbon	gel electrolyte with 5 M LiTFSI solution	2.5 V	-54°C	241.3 F g^{-1} single electrode	156.1 F g^{-1} single electrode	64.69%	-	-	5
activated carbon	cholinium chloride aqueous solutions (5 m)	1.5 V	-40°C	126 F g^{-1} single electrode	106 F g^{-1} single electrode	82.13%	-	-	6
$Co(OH)_2$ and activated carbon	$NaClO_4$ (9 M) and NaOH (1 M)	1.4 V	-30 °C	-	-	-	-	96.5% after 500 cycles	7
graphene	Li_2SO_4/ethylene glycol/water electrolyte	1.0 V	-20°C	91 F g^{-1} (1 mA cm^{-2}) single electrode	74 F g^{-1} (1 mA cm^{-2}) single electrode	81.32%	25.67% (from 1 to 10 mA cm^{-2})	-	8
activated carbon	Li_2SO_4 in water/methanol (7:3 v:v)	1.6 V	-40°C	87 F g^{-1} (0.2 A g^{-1}) single electrode	72 F g^{-1} (0.2 A g^{-1}) single electrode	82.76%	-	-	9

carbon nanotubes	$CaCl_2$ in FA/H_2O (1:1 v:v)	1.0 V	-60℃	107.6 F g^{-1} (100 mV s^{-1}) single electrode	72.7 F g^{-1} (100 mV s^{-1}) single electrode	67.57%	-	-	10
δ-MnO_2/activated carbon	5 M $NaClO_4$ in the methanol/water (1:5.2 m:m)	1.8 V	-35℃	47.4 F g^{-1} (0.25 A g^{-1})	42 F g^{-1} (0.25 A g^{-1})	88.60 %	-	-	11
activated carbon	5m LiTFSI-based hybrid electrolyte	2.2 V	-30℃	27 F g^{-1} (1 A g^{-1}) device	22 F g^{-1} (1 A g^{-1}) device	81.48%	40.91% (from 1 to 10 A g^{-1})	-	12
carbon nanotube paper	PVA/LiCl/H_2O/EG gel electrolyte	1.0 V	-40℃	~16 mF cm^{-2} device	~11.3 mF cm^{-2} device	70.60%	-	88.3% after 5000 cycle at -20 ℃	13
NiO and activated carbon	PVA/KOH/H_2O gel electrolyte	1.6 V	-20℃	61.5 F g^{-1} (0.1 A g^{-1}) device	41.4 F g^{-1} (0.1 A g^{-1}) device	67.32%	60% (from 0.1 to 1 A g^{-1})	72% after 800 cycles	14
BC-RGO	PA/KOH/H_2O gel electrolyte	1.0 V	-30℃	175 F g^{-1} (1 A g^{-1}) single electrode	75 F g^{-1} (1 A g^{-1}) single electrode	42.86%	-		15
NiO	4 M KOH containing $Fe(CN)_6^{3-}$/$Fe(CN)_6^{4-}$ couple	0.6 V	-20℃	-	128 F g^{-1} (2 A g^{-1}) single electrode	-	80% (from 0.5 to 2 A g^{-1})	96.4% after 1000 cycles	16
activated carbon	PPD in 38% H_2SO_4 solution	1.5 V	-18℃	-	-	-	-	-	17
NiO/ activated carbon, activated carbon	6 M KOH	1.5 V	-18℃	-	28.3 F g^{-1} (2.5 A g^{-1}) device	-	74% (from 1 to 2.5A g^{-1})	94% after 1000 cycles	18
CoNiFe ternary hydroxides	6 M KOH	0.45 V	-20℃	-	985 F g^{-1} (1.5 A g^{-1}) single electrode	-	-	76.9% after 500 cycles	19

TiC@PPy/PVA	6 M $NaNO_3$	1.4 V	-18℃	-	550 F g^{-1} (2 mV s^{-1}) single electrode	-	70% (from 2 to 400 mV s^{-1})	~70% after 5000 cycles	20
activated carbon/ 2-pyridinethiol	H_2SO_4 /H_2O/EG gel electrolyte	1.0 V	-40℃	309 F/g (5 mV s^{-1}) single electrode	108F/g (5 mV s^{-1}) single electrode	35%	-	-	21
activated carbon	crystal-type NaAc gel electrolyte	1.0 V	-40℃	175.9 F g^{-1} (1 A g^{-1}) single electrode	129.7 F g^{-1} (1 A g^{-1}) single electrode	73.73%	-	75.3% after 10000 cycles at -20℃	22
activated carbon	20 m LiTFSI electrolyte	2.4 V	-20℃	50 F g^{-1} (0.5 A g^{-1}) device	26 F g^{-1} (0.5 A g−1) device	52%	30.8% (from 0.5 to 2A g-1)	-	23
graphene	2M H_2SO_4 /DSMO/H_2O gel electrolyte	0.8 V	-50℃	161F g^{-1} (1 A g^{-1}) single electrode	161F g^{-1} (1 A g^{-1}) single electrode	~50%	-	-	24
activated carbon	**8.18 m $NaClO_4$-based hybrid electrolyte**	**2.3 V**	**-50 ℃**	**31.8 F g^{-1} (20 mV s^{-1}) device**	**27.5 F g^{-1} (20 mV s^{-1}) device**	**86.5%**	**78.2%** (from 10 to 100 mV s^{-1})	**91% after 120 h (~7000 cycles)**	**This work**

Table S3. The temperature dependence of specific capacitance, rate capability, R_i, R_{ct}, and relaxation time constant for supercapacitor based on YP-50F active material and $(NaClO_4)_{1.7}/(H_2O)_{4.7}(ACN)_3$ solution.

Temperature (°C)	20	0	-20	-40	-50
Specific Capacitance (F g^{-1})	31.8	30.9	30.2	28.8	27.5
Rate Capability (%)	92.1	93.1	92.2	85.4	78.2
R_i (Ω)	1.03	1.32	1.98	5.68	11.5
R_{ct} (Ω)	1.55	1.90	2.86	6.47	12.3
τ_0 (s)	0.83	1.21	1.78	4.65	10.0

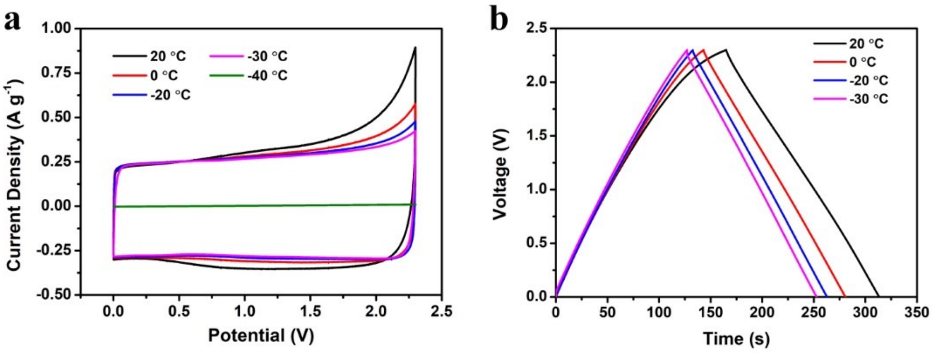

Figure S1. (a) The CV curves and (b) GCD curves of the supercapacitor based on 17 m $NaClO_4$ electrolyte at various temperatures.

As shown in Fig. S1a, when the operating temperature drops to -40 ℃, the current response in the CV curve is almost zero, indicating the failure of the device. The highly concentrated salt in the WIS electrolyte inevitably precipitates on surface of electrode material and separator at low temperatures, which blocks ions transfer, resulting in the failure of the supercapacitor ultimately at -40 ℃.

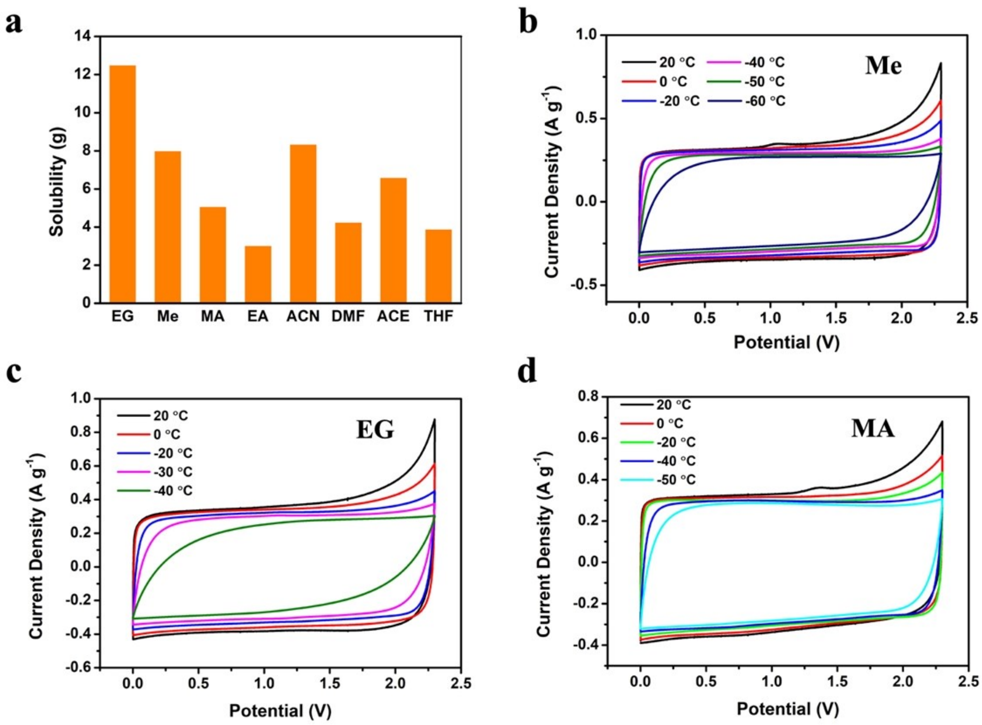

Figure S2. (a) The solubility of $NaClO_4$ in ethylene glycol (EG), methyl alcohol (Me), methyl acetate (MA), ethyl acetate (EA), acetonitrile (ACN), dimethylformamide (DMF), acetone (ACE) and tetrahydrofuran (THF). The mass of each organic solvent is 10 g. (b) The CV curves of supercapacitor based on active carbon and $(NaClO_4)_{1.7}/(H_2O)_{4.7}(Me)_3$ solution at various temperatures. (c) The CV curves of supercapacitor based on active carbon and $(NaClO_4)_{1.7}/(H_2O)_{4.7}(EG)_3$ solution at various temperatures. (d) The CV curves of supercapacitor based on active carbon and $(NaClO_4)_{1.7}/(H_2O)_{4.7}(MA)_3$ solution at various temperatures.

Besides previously reported ACN, other organic solvents, such as EG, Me, MA, EA, DMF, ACE and THF, also can dissolve $NaClO_4$ easily. We speculate these organic solvents would also have similar effect as ACN on suppressing salt precipitation in highly concentrated solution. We choose Me, EG and MA as co-solvent to prepare the hybrid electrolyte in the form of $(NaClO_4)_{1.7}/(H_2O)_{4.7}$(co-solvent)$_3$. The as-prepared electrolytes using Me, EG and MA as co-solvent still exhibit excellent electrochemical performance at subzero temperature.

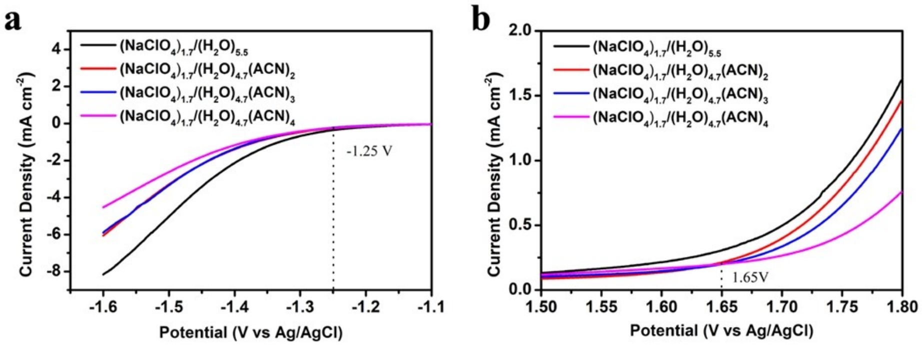

Figure S3. Magnified view of the regions near (a) cathodic and (b) anodic limits for $NaClO_4$-based solutions with different H_2O/ACN molar ratio. In this system, a value of 0.2 mA cm^{-2} was defined as the threshold for electrolyte decomposition.

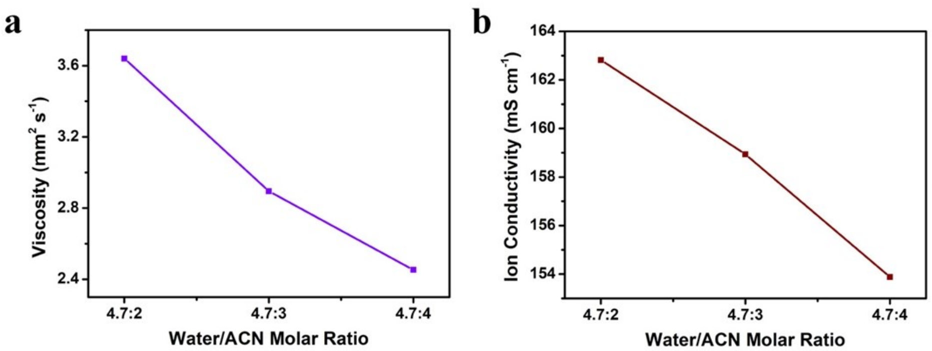

Figure S4. (a) Viscosities and (b) ionic conductivities of $NaClO_4$-based solutions with different H_2O/ACN molar ratio at room temperature.

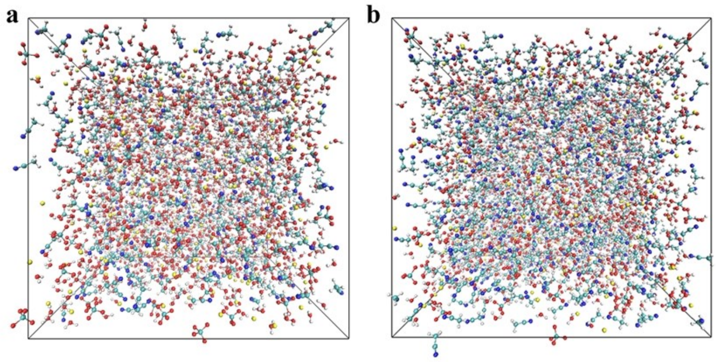

Figure S5. The MD simulation snapshots for (a) $(NaClO_4)_{1.7}/(H_2O)_{4.7}(ACN)_2$ solution, and (b) $(NaClO_4)_{1.7}/(H_2O)_{4.7}(ACN)_4$ solution.

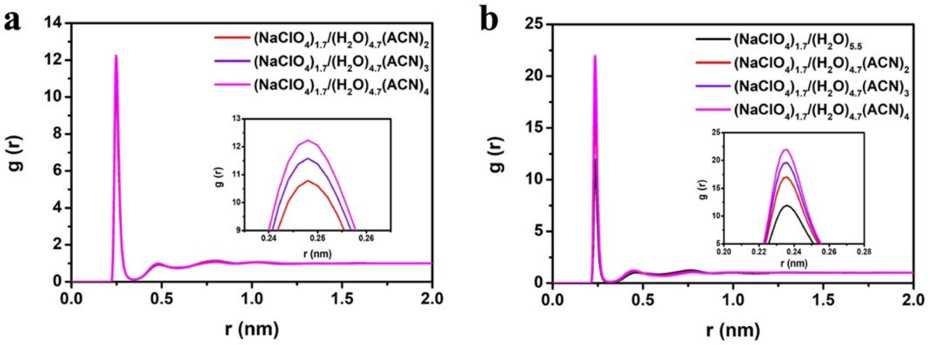

Figure S6. The RDF for (a) Na-N※, and (b) Na-O= of $NaClO_4$-based solutions with different H_2O/ACN molar ratio. N※ stands for N atom in ACN, and O= stands for O atom in H_2O.

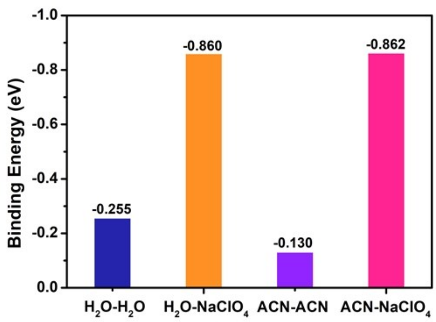

Figure S7. The binding energies of H_2O-H_2O, H_2O-$NaClO_4$, ACN-ACN, and ACN-$NaClO_4$.

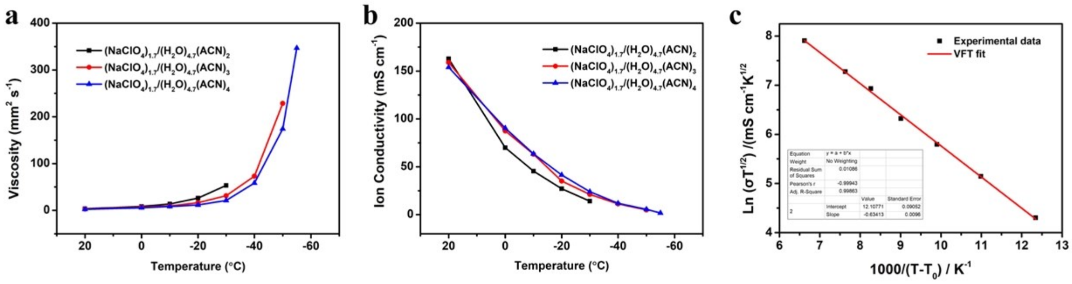

Figure S8. (a)The viscosities and (b)ion conductivities of the three hybrid solutions at various temperatures. (c)The ion conductivity of $(NaClO_4)_{1.7}/(H_2O)_{4.7}(ACN)_3$ solution at various temperatures.

The measured ionic conductivity of $(NaClO_4)_{1.7}/(H_2O)_{4.7}(ACN)_3$ solution was fitted by the Vogel–Tammann–Fulcher (VTF) empirical equation. The equation is described as follow.[25, 26]

$$\sigma(T) = AT^{-1/2}\exp(-E_a/R(T-T_0)) \tag{1}$$

Where $\sigma(T)$ is the ionic conductivity; A is the pre-exponential factor; E_a is the activation energy; R is the ideal gas constant, and T_0 is the ideal glass transition temperature.

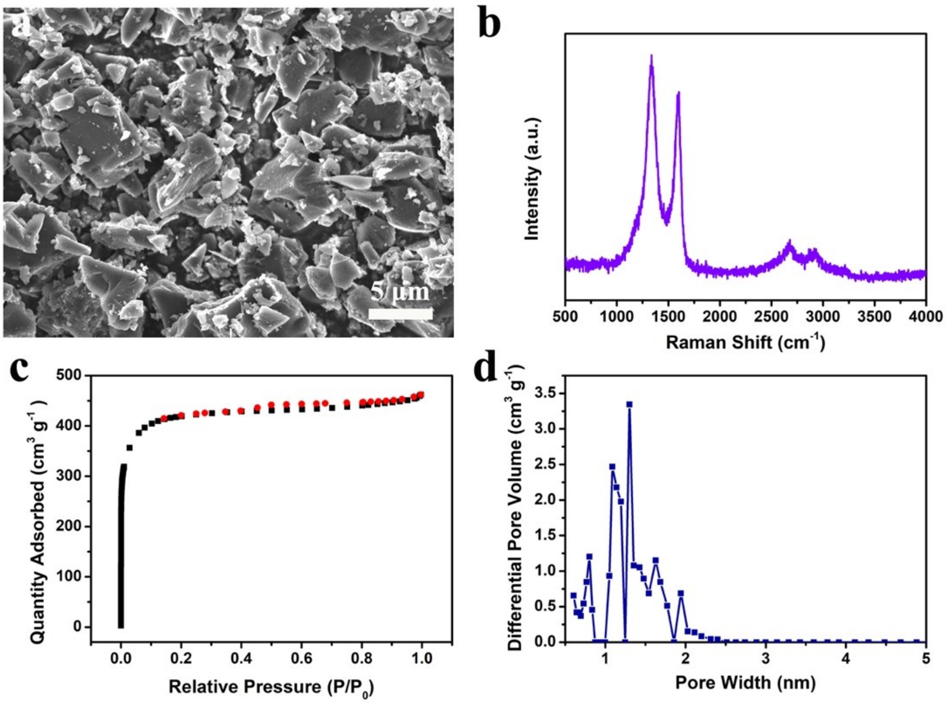

Figure S9. The characterization of commercial active carbon (YP-50F). ((a) The scanning electron microscope image of YP-50F. (b) The Raman spectrum of YP-50F. (c) The nitrogen adsorption-desorption isotherms of YP-50F. (d) The pore-size distribution of YP-50F.

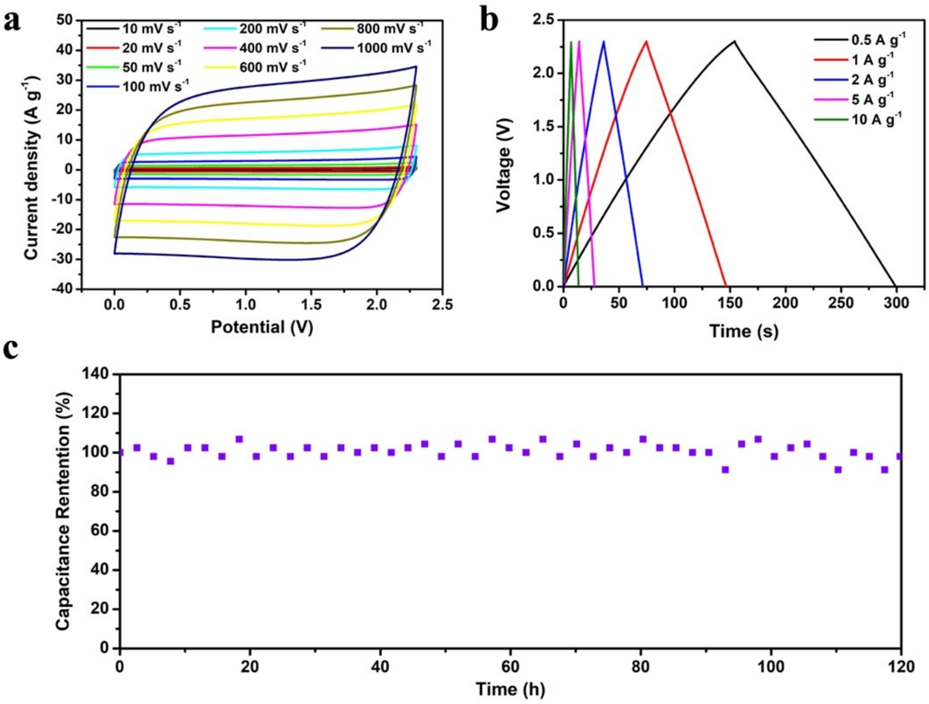

Figure S10. The electrochemical performance of supercapacitor based on active carbon and $(NaClO_4)_{1.7}/(H_2O)_{4.7}(ACN)_3$ solution at 20 °C. (a) The CV curves of supercapacitor at different scan rates. (b) The GCD curves of supercapacitor at different current densities. (c) The cycling stability of supercapacitor at the current density of 2 A g^{-1}.

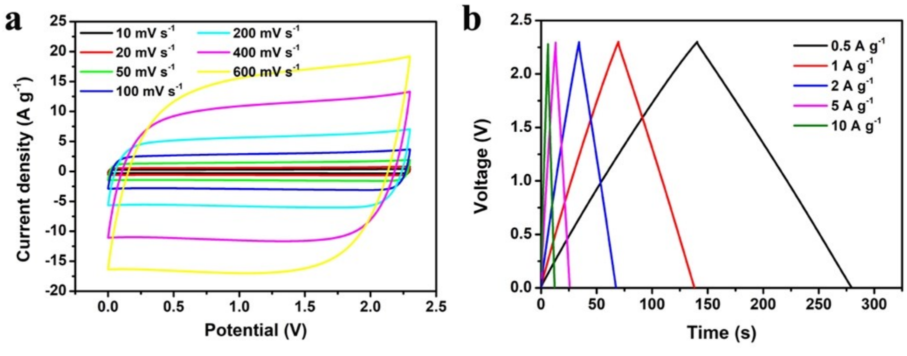

Figure S11. CV curves at various scan rates (a) and GCD curves at various current densities (b) for supercapacitor based on active carbon and $(NaClO_4)_{1.7}/(H_2O)_{4.7}(ACN)_3$ solution measured at -20 °C.

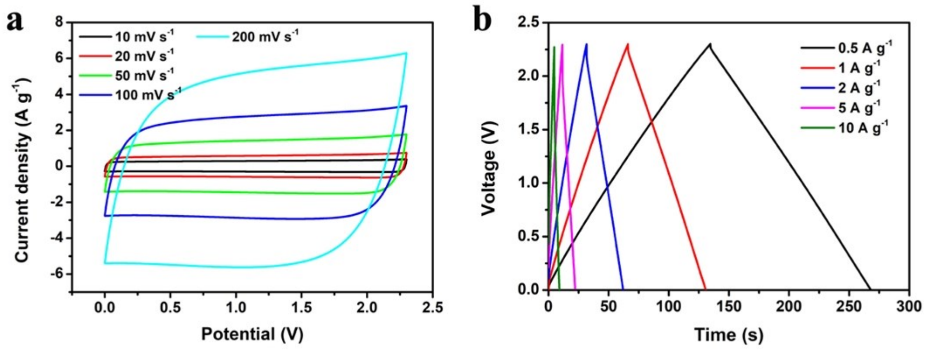

Figure S12. CV curves at various scan rates (a) and GCD curves at various current densities (b) for supercapacitor based on active carbon and $(NaClO_4)_{1.7}/(H_2O)_{4.7}(ACN)_3$ solution measured at -40 °C.

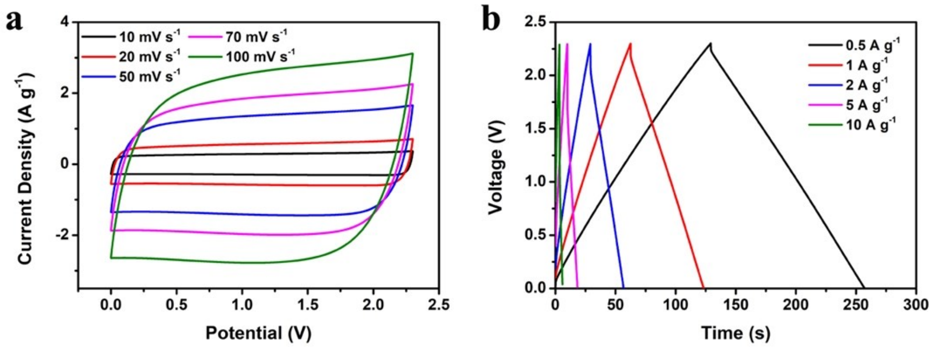

Figure S13. CV curves at various scan rates (a) and GCD curves at various current densities (b) for supercapacitor based on active carbon and $(NaClO_4)_{1.7}/(H_2O)_{4.7}(ACN)_3$ solution measured at -50 °C.

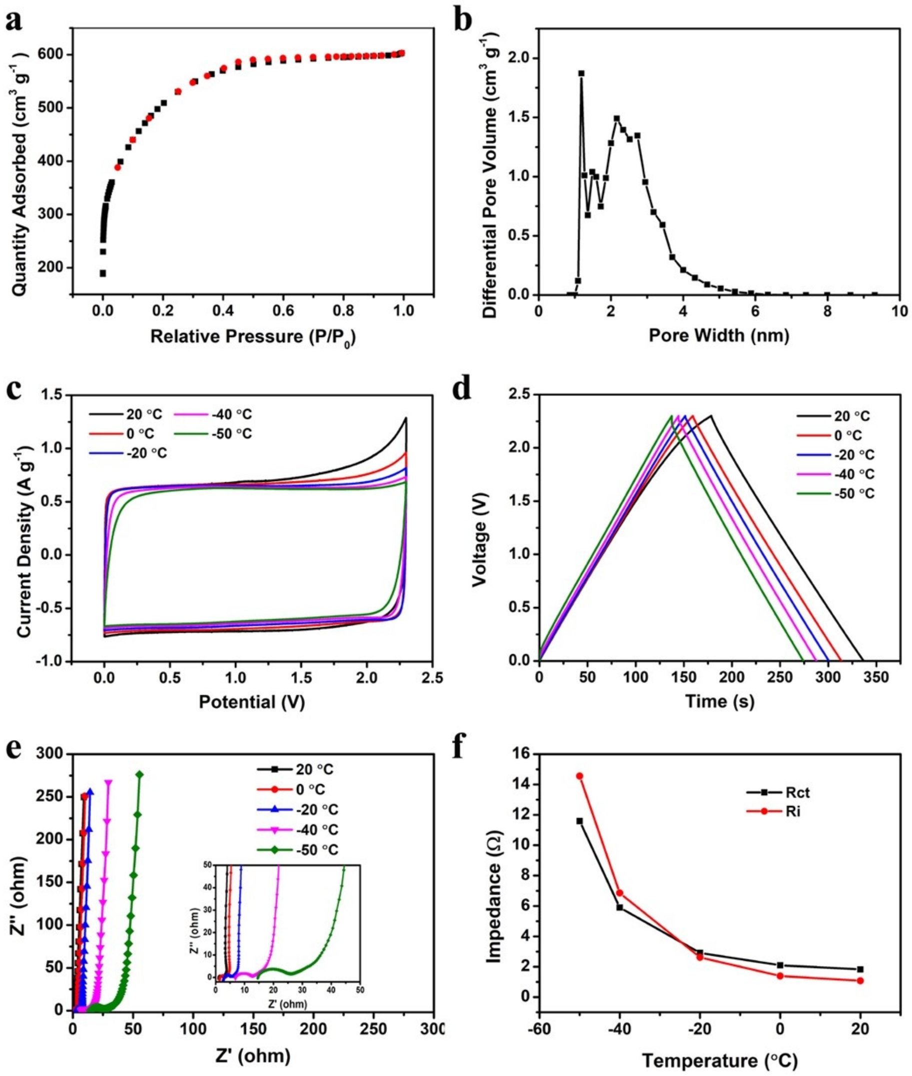

Figure S14. (a) The nitrogen adsorption-desorption isotherms of salt-templated carbon material (STC). (b) The pore-size distribution of STC. (c) The CV curves of supercapacitor based on STC at 20 mV s^{-1} at various temperatures. (d) The GCD curves of supercapacitor based on STC at 0.5A g^{-1} at various temperatures (e) The electrochemical impedance spectroscopy at various temperatures. (f) The internal resistance (R_i) and charge transfer resistance (R_{ct}) at various temperatures.

Reference

1. F. Tao, L. Qin, Z. Wang and Q. Pan, *ACS Appl. Mater. Interfaces*, 2017, **9**, 15541-15548.
2. Z. Wang, J. Cheng, J. Zhou, J. Zhang, H. Huang, J. Yang, Y. Li and B. Wang, *Nano Energy*, 2018, **50**, 106-117.
3. J. Yin, C. Zheng, L. Qi and H. Wang, *J. Power Sources*, 2011, **196**, 4080-4087.
4. A. Tatlisu, Z. Huang and R. Chen, *ChemSusChem*, 2018, **11**, 3899-3904.
5. J. Zhou, D. Wu, C. Wu, G. Wei, J. Wei, Z. Tai, S. Xi, S. Shen, Q. Wang and Y. Chen, *J. Mater. Chem. A*, 2019, **7**, 19753-19760.
6. Q. Abbas and F. Béguin, *ChemSusChem*, 2018, **11**, 975-984.
7. T. Deng, W. Zhang, H. Zhang and W. Zheng, *Energy Technol.*, 2018, **6**, 605-612.
8. R. Vellacheri, A. Al-Haddad, H. Zhao, W. Wang, C. Wang and Y. Lei, *Nano Energy*, 2014, **8**, 231-237.
9. Q. Abbas and F. Béguin, *J. Power Sources*, 2016, **318**, 235-241.
10. Y. Gao, Z. Qin, L. Guan, X. Wang and G. Z. Chen, *Chem. Commun.*, 2015, **51**, 10819-10822.
11. L. Chen, H. Li, H. Yoshitake, L. Qi, N. Gu and H. Wang, *Electrochim. Acta*, 2015, 157, 333-344.
12. Q. Dou, S. Lei, D.-W. Wang, Q. Zhang, D. Xiao, H. Guo, A. Wang, H. Yang, Y. Li, S. Shi and X. Yan, *Energy Environ. Sci.*, 2018, **11**, 3212-3219.
13. Q. Rong, W. Lei, J. Huang and M. Liu, *Adv. Energy Mater.*, 2018, **8**, 1801967.
14. C. Yuan, X. Zhang, Q. Wu and B. Gao, *Solid State Ionics*, 2006, **177**, 1237-1242.
15. X. Li, L. Liu, X. Wang, Y. S. Ok, J. A. W. Elliott, S. X. Chang and H. J. Chung, *Sci. Rep.*, 2017, **7**, 1685.
16. L. Su, L. Gong and Y. Zhao, *Phys. Chem. Chem. Phys.*, 2014, **16**, 681-684.
17. L. Su, L. Gong, C. Ma, X. Wang and Z. Sun, *ChemElectroChem*, 2017, **4**, 46-48.
18. L. Su, L. Gong, X. Wang and H. Pan, *Int. J. Energy Res.*, 2016, **40**, 763-769.
19. L. Su, Z. Song, J. Guo and J. Li, *ChemistrySelect*, 2017, **2**, 2665-2669.
20. Y.-T. Weng, H.-A. Pan, N.-L. Wu and G. Z. Chen, *J. Power Sources*, 2015, **274**,

1118-1125.

21. Y. Shang, J. Wei, C. Wu and Q. Wang, *ACS Appl. Mater. Interfaces*, 2018, **10**, 42959-42966.

22. J. Wei, G. Wei, Y. Shang, J. Zhou, C. Wu and Q. Wang, *Adv. Mater.*, 2019, **31**, e1900248.

23. S.-W. Xu, M.-C. Zhang, G.-Q. Zhang, J.-H. Liu, X.-Z. Liu, X. Zhang, D.-D. Zhao, C.-L. Xu and Y.-Q. Zhao, *J. Power Sources*, 2019, **441**, 227220.

24. C. Lu and X. Chen, *Nano Lett.*, 2020, **20**, 1907-1914.

25. F. Croce, M. L. Focarete, J. Hassoun, I. Meschini and B. Scrosati, *Energy Environ. Sci.*, 2011, **4**, 921-927.

26. X. Fan, X. Ji, L. Chen, J. Chen, T. Deng, F. Han, J. Yue, N. Piao, R. Wang, X. Zhou, X. Xiao, L. Chen and C. Wang, *Nat. Energy*, 2019, **4**, 882-890.